ADVANCED FUNCTIONAL MATERIALS
www.afm-journal.de

# Tissue Engineered Bio-Blood-Vessels Constructed Using a Tissue-Specific Bioink and 3D Coaxial Cell Printing Technique: A Novel Therapy for Ischemic Disease

*Ge Gao, Jun Hee Lee, Jinah Jang, Dong Han Lee, Jeong-Sik Kong, Byoung Soo Kim, Yeong-Jin Choi, Woong Bi Jang, Young Joon Hong,* Sang-Mo Kwon,* and Dong-Woo Cho**

**Endothelial progenitor cells (EPCs) are a promising cell source for the treatment of several ischemic diseases for their potentials in neovascularization. However, the application of EPCs in cell-based therapy has shown low therapeutic efficacy due to hostile tissue conditions after ischemia. In this study, a bio-blood-vessel (BBV) is developed, which is produced using a novel hybrid bioink (a mixture of vascular-tissue-derived decellularized extracellular matrix (VdECM) and alginate) and a versatile 3D coaxial cell printing method for delivering EPC and proangiogenic drugs (atorvastatin) to the ischemic injury sites. The hybrid bioink not only provides a favorable environment to promote the proliferation, differentiation, and neovascularization of EPCs but also enables a direct fabrication of tubular BBV. By controlling the printing parameters, the printing method allows to construct BBVs in desired dimensions, carrying both EPCs and atorvastatin-loaded poly(lactic-*co*-glycolic) acid microspheres. The therapeutic efficacy of cell/drug-laden BBVs is evaluated in an ischemia model at nude mouse hind limb, which exhibits enhanced survival and differentiation of EPCs, increased rate of neovascularization, and remarkable salvage of ischemic limbs. These outcomes suggest that the 3D-printed ECM-mediated cell/drug implantation can be a new therapeutic approach for the treatment of various ischemic diseases.**

## 1. Introduction

Endothelial progenitor cells (EPCs) are a promising cell source for the treatment of several ischemic diseases for their potentials in neovascularization.[1] Nevertheless, the hostile ischemic conditions (e.g., low nutrition, oxidative stress, inflammation, reactive oxygen species) limit survival and differentiation of transplanted EPCs, and thus result in low therapeutic efficacy.[2] Atorvastatin, a hydroxymethylglutaryl-coenzyme A reductase inhibitor, has exhibited good abilities to mobilize EPCs,[3] enhances angiogenesis by reducing subdural hematoma,[4] and promotes endothelial cells function.[5] However, an efficient method for coupling the therapeutic effects of atorvastatin and EPCs is still unmet.

Tissue engineering can provide solutions since it converges the usage of cells, biomaterials, and biological factors to restore or replace the disorders. In particular,

G. Gao, B. S. Kim, Prof. D.-W. Cho
Department of Mechanical Engineering
Pohang University of Science and Technology
Pohang 37673, Republic of Korea
E-mail: dwcho@postech.ac.kr
Dr. J. H. Lee
Department of Pharmacology and Toxicology
University of Alabama at Birmingham School of Medicine
Birmingham, AL 35294, USA
Prof. J. Jang
Department of Creative IT Engineering
Pohang University of Science and Technology
Pohang 37673, Republic of Korea
D. H. Lee, W. B. Jang
Laboratory for Vascular Medicine and Stem Cell Biology
Medical Research Institute
Department of Physiology
School of Medicine
Pusan National University
Yangsan 626-870, Republic of Korea
J.-S. Kong
School of Interdisciplinary Bioscience and Bioengineering
Pohang University of Science and Technology
Pohang 37673, Republic of Korea
Y.-J. Choi
Division of Integrative Biosciences and Biotechnology
Pohang University of Science and Technology
Pohang 37673, Republic of Korea
Prof. Y. J. Hong
Heart Center of Chonnam National University Hospital
Gwangju 501-757, Republic of Korea
E-mail: hyj200@hanmail.net
Prof. S.-M. Kwon
Laboratory for Vascular Medicine and Stem Cell Biology
Medical Research Institute
Department of Physiology
School of Medicine
Immunoregulatory Therapeutics Group in Brain Busan 21 Project
Pusan National University
Yangsan 626-870, Republic of Korea
E-mail: smkwon323@pusan.ac.kr

DOI: 10.1002/adfm.201700798

© 2017 The Authors. Published by WILEY-VCH Verlag GmbH & Co. KGaA, Weinheim. This is an open access article under the terms of the Creative Commons Attribution-NonCommercial-NoDerivatives License, which permits use and distribution in any medium, provided the original work is properly cited, the use is non-commercial and no modifications or adaptations are made.

The copyright line of this paper was changed 17 August 2017 after initial publication.

3D cell printing is regarded as a versatile technique for tissue engineering due to the high freedom for positioning cells and biomolecules in a wide range of biomaterials with predesigned patterns and geometries.[6] Particularly, 3D coaxial cell printing has shown potentials for vascular tissue engineering because of the ability of directly fabricating perfusable vessel-mimicking structure by extruding cell-laden biomaterials through a coupled core/shell nozzle.[7] In this technique, one indispensable requirement for biomaterial is instant gelation behavior. Therefore, alginate-based hydrogel is widely used due to the rapid ionic crosslinking via calcic treatment.[7,8] However, the deficiency of binding sites for cell attachment and migration in alginate drastically impairs activities of entrapped cells. Hence, it is necessary to seek an endothelial-inspiring material for this engineering technique.

Tissue-specific decellularized extracellular matrices (dECMs) have demonstrated the superiorities in mediating cellular functions compared with other prevalent biomaterials.[9] Because, they can uniquely recapitulate the inherent microenvironments of original tissue including composition, structure, and biomechanical properties, which are critical regulators of cell fates such as survival, maturation, differentiation, and migration. In our previous studies, a variety of tissue derived dECMs (e.g., adipose, cartilage, cardiac, muscle, and liver) have been successfully formulated as printable bioink.[10] Combining with 3D cell printing technique to modulate cell alignment and control graft structure, the dECM-based tissue analogues have achieved promoted cell activities, enhanced tissue functions, and accelerated therapeutic effects.[10b,d] Therefore, we believe that a vascular-tissue-derived dECM (VdECM) bioink can compensate the drawback of alginate to both enable the direct tube printing and improve cell functions, and thus helps to produce biofunctional structure.

In this study, we engineered a EPC/atorvastatin-loaded poly(lactic-*co*-glycolic) acid (PLGA) microspheres (APMS) laden bio-blood-vessel (BBV) by combining 3D coaxial cell printing technique and a hybrid bioink composed of VdECM and alginate (**Figure 1**A,B). The in vitro evaluations of hybrid bioink revealed enhanced cell viability, proliferation, differentiation of EPCs compared with type-I collagen. In addition, the hybrid bioink enabled a direct fabrication of cell/drug laden tubes with

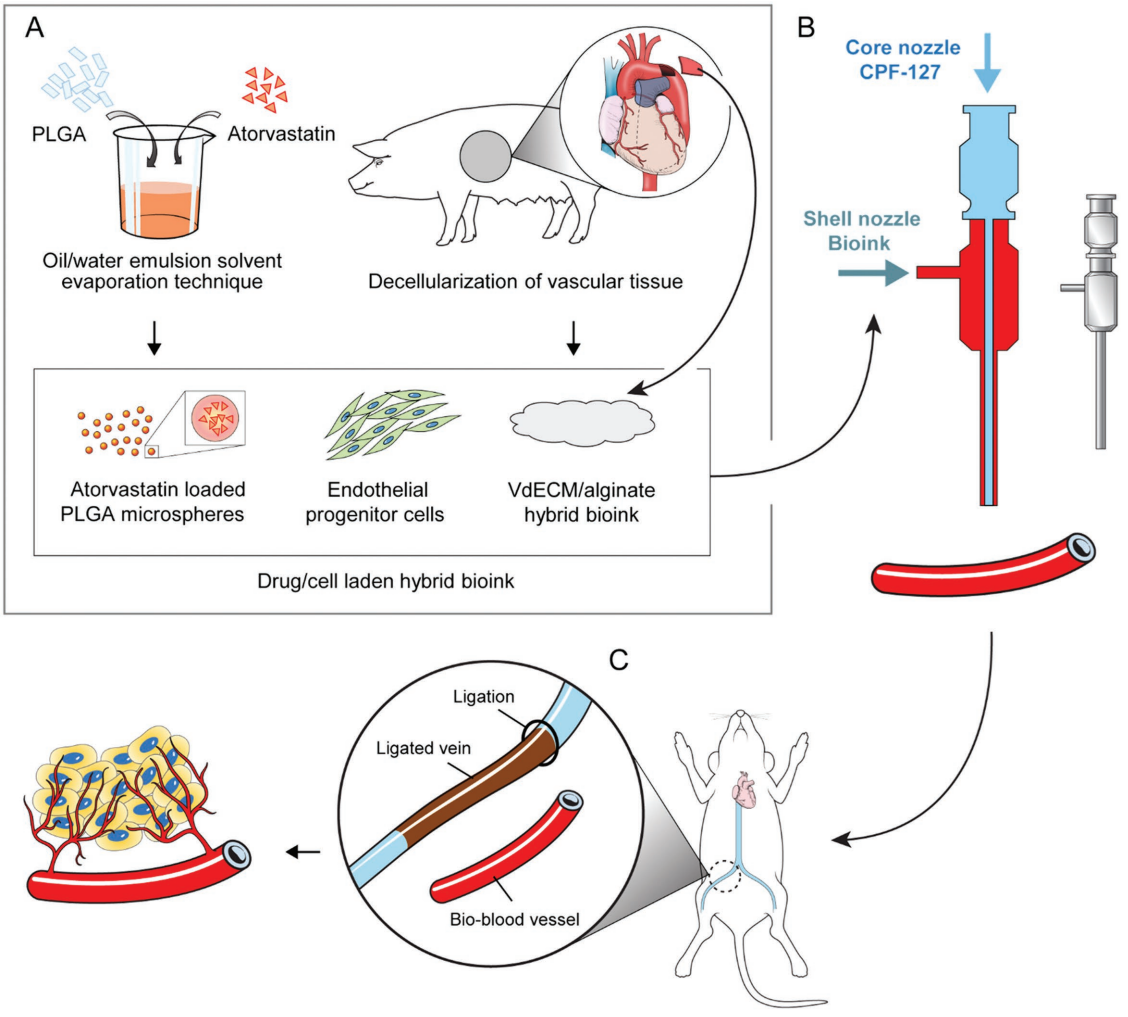


**Figure 1.** Schematic of research strategy. A) A hybrid bioink was prepared by mixing VdECM and sodium alginate, which was used to encapsulate the atorvastatin/PLGA microspheres and endothelial progenitor cells. B) A 3D coaxial printing technique was applied to construct the cell/drug-laden BBV. C) The fabricated BBV was evaluated in a mouse model by transplanting the structure to the vicinity of the ligated limb vein to treat ischemic disease.


© 2017 The Authors. Published by WILEY-VCH Verlag GmbH & Co. KGaA, Weinheim

varied dimensions by modulating the printing parameters. Moreover, the observed in vitro endothelialization of perfusable BBV demonstrated its significant potentials to develop functional blood vessel graft. The therapeutic efficacy of BBV was investigated in a nude mice hind limb ischemia model (Figure 1C). The significantly improved performance of EPCs and promoted recovery rate of ischemic injury proved the superior therapeutic effects of such a BBV-based method compared to conventional cell and drug treatments.

## 2. Results

### 2.1. Evaluation of a Hybrid Bioink

The preparation of our hybrid bioink required that we first attained VdECM from porcine aortic tissue using a series of physical, chemical, and enzymatic decellularizing treatments, which drastically eliminated DNA content (4.92 ± 0.63%) while preserving the majority of ECM components such as collagen (135.29 ± 6.86%), glycosaminoglycans (GAG) (75.89 ± 2.74%), and elastin (60.39 ± 7.09%) in the original tissue (Figure S1, Supporting Information). The recipe of the hybrid bioink was optimized using the minimal concentration achieving BBV fabrication, a 2% (w/v) ratio of alginate in hybrid bioink. For determining the concentration of VdECM in hybrid bioink, we tested the proliferation rate of EPCs in response to each hybrid bioink combination, including 2% (w/v) alginate coupled with 2% (w/v), 3% (w/v), and 4% (w/v) VdECM (2V2A, 3V2A, 4V2A) (Figure S2, Supporting Information). Although it possessed a higher concentration of VdECM, the performance of 4V2A was slightly inferior to that of 3V2A. One possible reason comes from the increased matrix stiffness when using a higher concentration of VdECM, as this may impede cell activities, such as cell migration and proliferation.[11] The 3V2A group was determined as the hybrid bioink for the subsequent experiments based on these analyses.

We assessed the performance of encapsulated EPCs including cell proliferation, viability, and differentiation to evaluate the biofunctionality of hybrid bioink. Positive controls were 3% w/v Type I collagen (COL) and 3% w/v VdECM, and 2% w/v alginate (ALG) was used as a negative control. The population of EPC in COL, VdECM, and hybrid bioinks expanded well over a week, but were significantly diminished in the ALG bioink (**Figure 2**A). The metabolic activities of living cells in VdECM and hybrid bioinks significantly surpassed those of the COL bioink after 4 d, which demonstrated their cell proliferation superiority. LIVE/DEAD cell assay indicated the distribution of cells in each bioink (Figure 2B). Notably, EPCs did not spread and many were dead in the alginate group after culturing for 7 d, which can explain its descending population of encapsulated EPCs as observed in the proliferation test. In contrast, the hybrid bioink promoted the viability and proliferation capability similar to COL and VdECM bioinks. Interestingly, EPCs formed the interconnected vessel-like structures in both the VdECM and hybrid bioinks, which is a distinctive feature unlike the merely stretched morphology in the COL bioink.

We hypothesized that the interaction between cells and their native ECM-component containing bioinks, such as VdECM and hybrid bioink, promotes the differentiation of EPCs and the formation of the vasculature based on the proliferation test results. We verified this hypothesis by conducting reverse transcription polymerase chain reaction (RT-PCR) on day 7 using three typical markers of endothelial cells, including CD31, VE-cadherin, and von Willebrand factor. The result revealed that the expression levels of relevant genes in the hybrid bioink were significantly improved compared to the COL bioink (Figure 2C). Furthermore, the results of immunofluorescence staining against CD31 identified the differentiation of EPCs into more mature endothelial cells and the microvessel formation of EPCs in VdECM and hybrid bioink at day 7. In contrast, collagen only achieved scarce cell aggregation (Figure 2D). In this sense, we demonstrated that the hybrid bioink potentially offered a favorable environment promoted cell adhesion, spreading, and differentiation.

A bioink should present appropriate rheological properties for fabricating a BBV to carry cells and drugs. Similar to the other bioinks, the hybrid bioink exhibited shear thinning behavior (Figure 2E), which benefited the viability of the entrapped cells due to the alleviated shear stress when passing through printing nozzles at a certain flow rate.[12] The crosslinked gel with greater storage modulus than loss modulus can retain its shape, and thus fulfill the fabrication of BBV (Figure 2F).

In addition, the scanning electron microscope (SEM) images unveiled that the crosslinked hybrid bioink possesses interconnected pores ranging from dozens to hundreds of microns (Figure S5A,D, Supporting Information), which allow cells to migrate, proliferate, and differentiate. Moreover, the micropores between fibers (Figure S5B,C, Supporting Information) can facilitate diffusion of oxygen, ions, and metabolites.

### 2.2. Determination of Effective Drug Concentration

The proliferation of EPCs was assessed after treatment with atorvastatin (0, $0.01 \times 10^{-6}$, $0.1 \times 10^{-6}$, and $1 \times 10^{-6}$ M) for 24 h (**Figure 3**A) to verify the effect of atorvastatin on proliferation of EPCs. Atorvastatin treatment augmented EPC proliferation, with the maximal effect being observed at $0.1 \times 10^{-6}$ M atorvastatin. In addition, the cell cycle-associated proteins (cyclin D1 and cyclin-dependent kinase 2, CDK2) of the EPCs were significantly increased in the treatment with atorvastatin compared to those without atorvastatin treatment (Figure 3B). Any drug treatment can adversely affect the function of stem/progenitor cells. In this regard, we examined the effects of atorvastatin on the EPC characteristics and their functionality using flow cytometry technique. Figure 3C shows no adverse or positive effect on both nonendothelial markers (CD11b, CD14, and CD45) and endothelial markers (CD31, CD144, Tie-2, and VEGFR2), indicating that atorvastatin does not affect the characteristic of EPCs (Figure 3C). The examinations were performed to investigate whether the atorvastatin could influence the performance of EPCs. In addition, migration assay validates that atorvastatin does not inhibit EPC migration (Figure 3D). These observations suggest that atorvastatin increases the proliferative potential of EPCs, but does not affect the fundamental characteristics of EPCs.


© 2017 The Authors. Published by WILEY-VCH Verlag GmbH & Co. KGaA, Weinheim

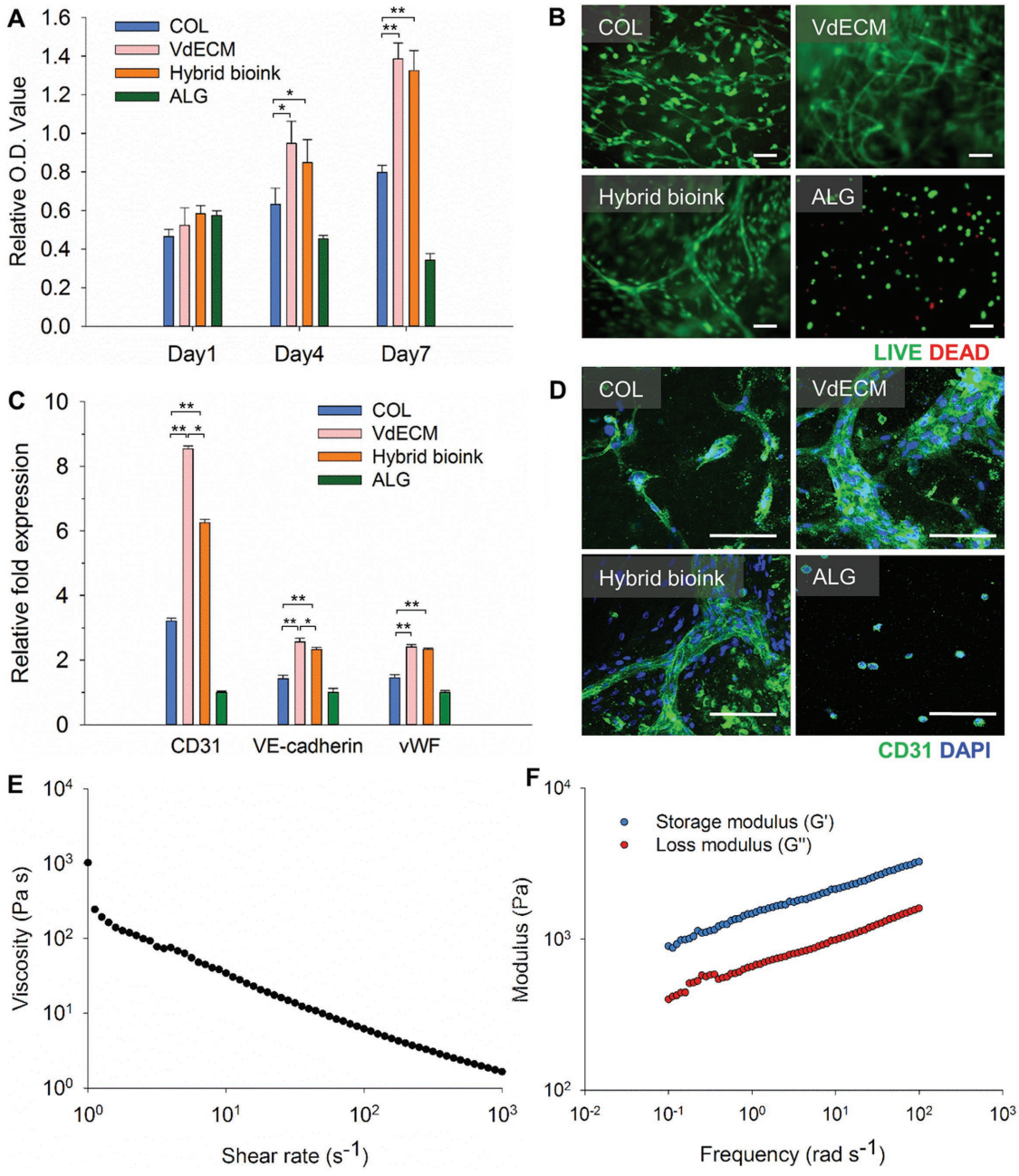


**Figure 2.** Evaluation of a hybrid bioink. A) EPCs encapsulated in the hybrid bioink showed a significantly higher proliferation rate than in COL (*, $p < 0.5$; **, $p < 0.005$). B) The few detected dead cells at day 7 proved that the hybrid bioink provides a friendly environment to EPCs to thus achieve high viability (Green: live cells and Red: dead cells; Scale bar: 100 µm). C) The hybrid bioink facilitated the gene expression of EPCs (*, $p < 0.5$, **; $p < 0.005$). D) The formation of vasculature in vitro was detected in hybrid bioink at day 7 by immunofluorescence staining (Green: CD31 and Blue: 4′6-diamidino-2-phenylindole (DAPI); Scale bar: 100 µm). E) The viscosity of hybrid bioinks that exhibited shear thinning behavior. F) The complex modulus of crosslinked hybrid bioinks indicated a higher storage modulus than loss modulus.

PLGA microspheres were selected as a secondary carrier for the drug to provide a sustained stimulating effect of atorvastatin to EPCs. Some studies have demonstrated microparticles prepared by polyhydroxy acid (e.g., polycaprolactone, polyglycolide, or PLGA) can prolong the release of encapsulated drugs over a month.[13] When exposed to the in vivo conditions, the autocatalytic effect of accumulated acidic products can facilitate the degradation of PLGA, and thus enables and promotes the release of atorvastatin to surroundings.[14] APMS were obtained through an oil/water emulsion solvent evaporation method, which allows us to approximately control the average diameter of microspheres at 10, 50, and 100 µm by adjusting the power of the homogenizer at 15 000, 7000, and 3000 rpm, respectively (Figure S3, Supporting Information). The small size of the microspheres gave them the tendency to induce rapid releasing kinetics.[15] In contrast, loading large ones might create a risk


© 2017 The Authors. Published by WILEY-VCH Verlag GmbH & Co. KGaA, Weinheim

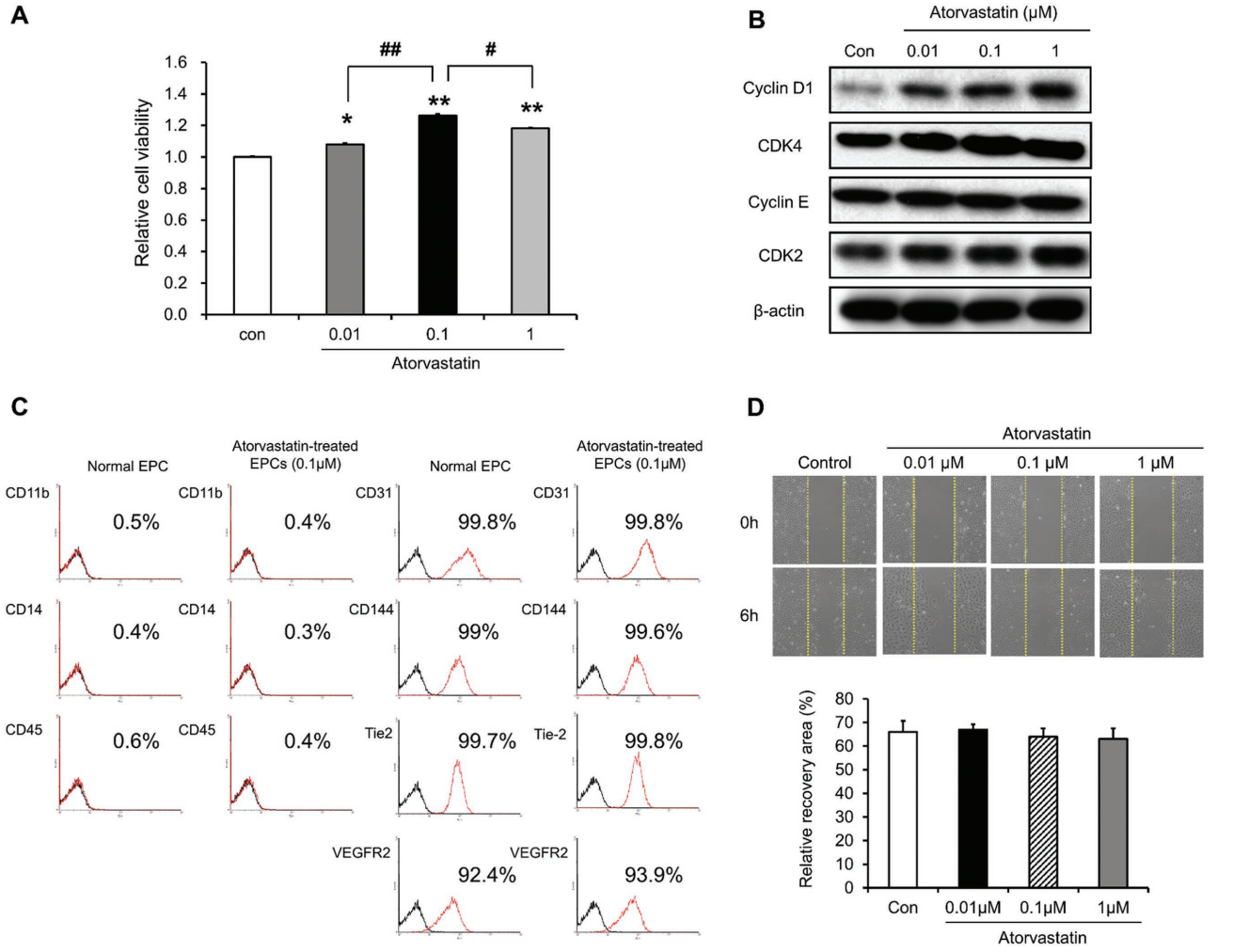


**Figure 3.** Assessment of effective drug concentration. A) EPCs were treated with atorvastatin (0, $0.01 \times 10^{-6}$, $0.1 \times 10^{-6}$, or $1 \times 10^{-6}$ M) for 24 h, after which the proliferation of EPCs was assessed. Values represent mean ± SEM. *, $p < 0.05$; **, $p < 0.01$ versus nontreated EPCs (con) and #, $p < 0.05$; ##, $p < 0.01$ versus atorvastatin-treated EPCs ($0.1 \times 10^{-6}$ M). B) After the treatment of EPCs with atorvastatin (0, $0.01 \times 10^{-6}$, $0.1 \times 10^{-6}$, or $1 \times 10^{-6}$ M) for 24 h, the expression of cell cycle-associated proteins (cyclin D1, CDK2, cyclin E, and CDK4) was assessed by western blot analysis. C) The surface markers of EPCs were detected by flow cytometry analysis for anti-CD11b, CD13, CD45, CD31, CD144, Tie2, and VEGFR2. Histograms represent the cell number (*y*-axis) versus the fluorescence intensity (*x*-axis, log scale). Flow cytometry analysis gating was performed using cells stained with isotype-matched IgG as a negative control. Black lines indicate the negative control cells and red lines indicate cells stained with each antibody. D) The migration of EPCs treated with atorvastatin (0, $0.01 \times 10^{-6}$, $0.1 \times 10^{-6}$, and $1 \times 10^{-6}$ M) was evaluated by scratched wound healing assay.

of nozzle blockage during the printing process. These prerequisites determined that APMS with an average diameter of 50 μm was appropriate in this study. This method and these determined parameters allowed us to produce APMS with the atorvastatin content of 10.35 ± 2.65%. In addition, the high hydrophobicity of APMS, due to the high ratio of polylactic acid to polyglycolic acid in the applied PLGA (with lactide:glycolide ratio of 85:15), could avoid the cell adhesion which might influence the interactions between EPCs and ECM.[14a,16]

### 2.3. Construction of Cell/Drug-Laden Bio-Blood-Vessel

We developed a fabrication process to attain tube-shaped BBV as cell/drug carriers using 3D coaxial printing technology (**Figure 4**A). The hybrid bioink encapsulating EPCs/APMS was loaded in the syringe for the shell nozzle and 40% w/v Pluronic F-127 dissolved in $100 \times 10^{-3}$ M $CaCl_2$ solution (CPF127) was filled in the syringe for the core nozzle. When these two materials encountered after being simultaneously deposited from related nozzles, the alginate within the hybrid bioink was ionically crosslinked by the $Ca^{2+}$ released from CPF127, and thus formed a tubular structure (the CPF127 both contributed to initiating the gelation of alginate in bioink by releasing $Ca^{2+}$ ions and supported avoiding the deformation of BBV prior to the VdECM crosslinking) (Figure 4A(i) and Movie S1 (Supporting Information)). Afterward, the printed tubular structure was incubated at 37 °C for 30 min to facilitate the thermal gelation of collagenous proteins in the VdECM (Figure 4A(ii)). Finally, hollow BBV was obtained by immersing the sample in culture medium for 10 min to dissolve and eliminate the water-soluble CPF127 (Figure 4A(iii) and Movie S2 (Supporting


© 2017 The Authors. Published by WILEY-VCH Verlag GmbH & Co. KGaA, Weinheim

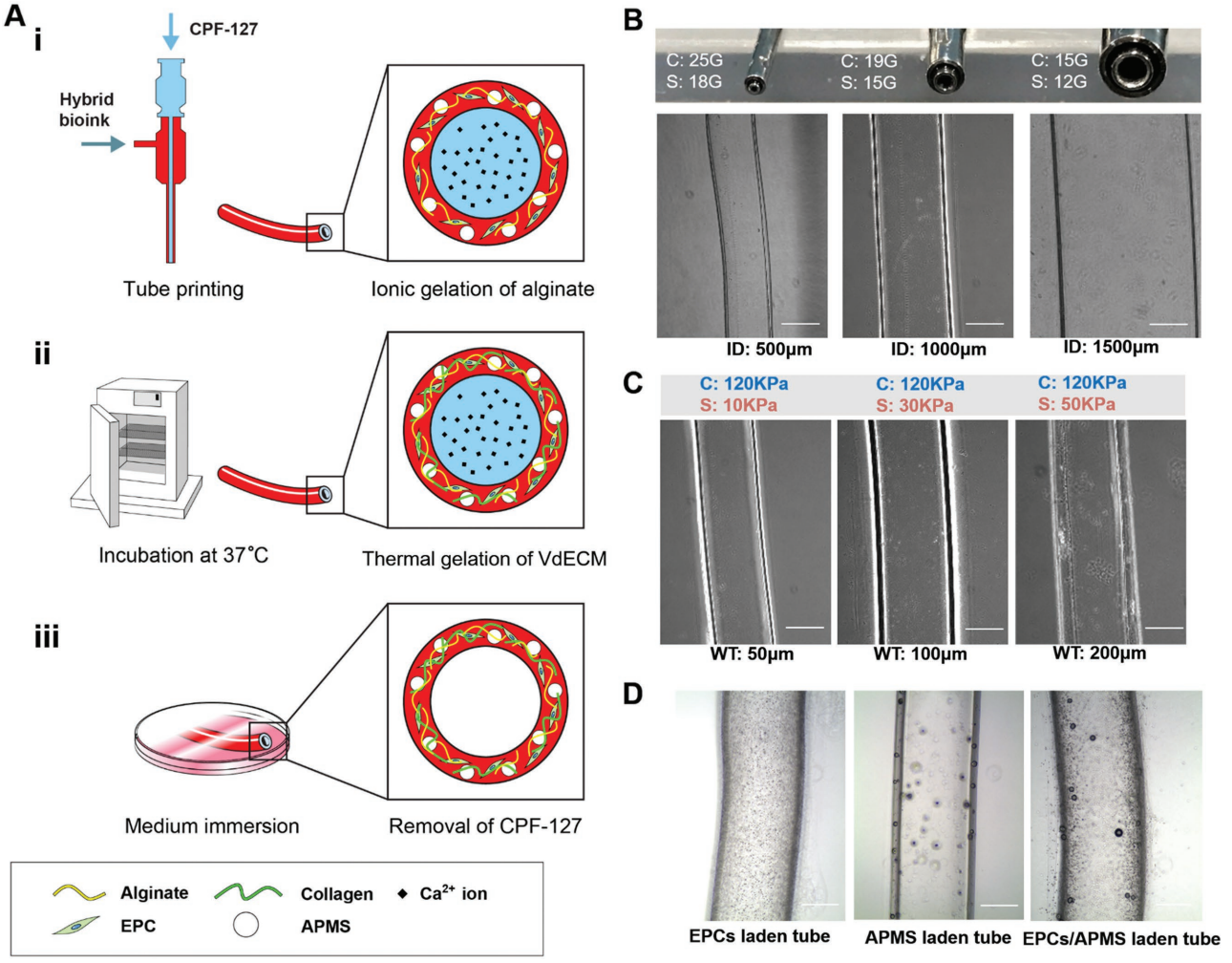


**Figure 4.** Fabrication and structural configuration of the BBVs. A) A schematic depiction of the BBV fabrication process. The ionic gelation of alginate in 3V2A realized BBV printing (i), the thermal crosslinking of collagen fibers was induced by incubation at 37 °C (ii), medium immersion dissolved and removed CPF127 to obtain BBV with a hollow tubular shape (iii). B) Combinations of various core and shell nozzles allowed the production of tubes with different inner diameters. C) Adjusting the flow rate of 3V2A in the shell nozzle (15/19 gauge) permitted the achievement of BBVs with different wall thicknesses. D) Using a 15/19 gauge coaxial nozzle permitted the successful fabrication of EPCs, AMPS, and EPC/AMPS laden BBVs (scale bar: 500 μm).

Information)). The BBV enabled perfusion through the hollow channel (Movie S3, Supporting Information).

The merit of 3D coaxial printing technology is the expediency with which the dimensions of the tubular constructs can be controlled by adjusting the printing parameters, such as the flow rate and the nozzle gauge. We fabricated various sizes of BBV by combining various pneumatic pressures and core/shell nozzle calibers. The inner diameter (ID) of the BBV can be adjusted in the range from 500 to 1500 μm using different sizes of coaxial nozzle (Figure 4B), and the wall thickness (WT) can be controlled in the range from 50 to 200 μm by changing the flow rates of the shell nozzle with a determined coaxial nozzle (Figure 4C). While a small ID and WT resulted in less amount of encapsulated cells and limited space in which to accommodate APMS (≈50 μm in diameter), a too large WT might induce the insufficient permeation of oxygen and nutrients.[17] These considerations suggest that we choose 1000 μm for the inner diameter and 100 μm for the wall thickness as the dimensions of the printed BBV for subsequent experiments. CPF127 and the hybrid bioink were, respectively, dispensed using a 19 gauge core nozzle with 120 kPa pneumatic pressure and a 15 gauge shell nozzle with 30 kPa pneumatic pressure to fabricate a BBV of such size. These printing parameters gave rise to the smooth fabrication of a bio-blood-vessel carrying both EPCs and APMS (Figure 4D).

Currently, the tissue engineered blood vessels could be developed using a variety of techniques (e.g., scaffold processing,[18] annular mode casting,[19] cell sheets,[20] and decellularization of arteries/vein).[21] Although the cell sheets based and decellularized vascular organ has been attempted for clinical application, the long-term preparation, low cost efficiency, and inflexible dimensions cannot match the critical demands of clinical trials.[22] Compared with these disadvantages, the versatility and flexibility of 3D coaxial cell printing technique exhibits the potentials to open a new avenue for engineering artificial blood vessels.


© 2017 The Authors. Published by WILEY-VCH Verlag GmbH & Co. KGaA, Weinheim

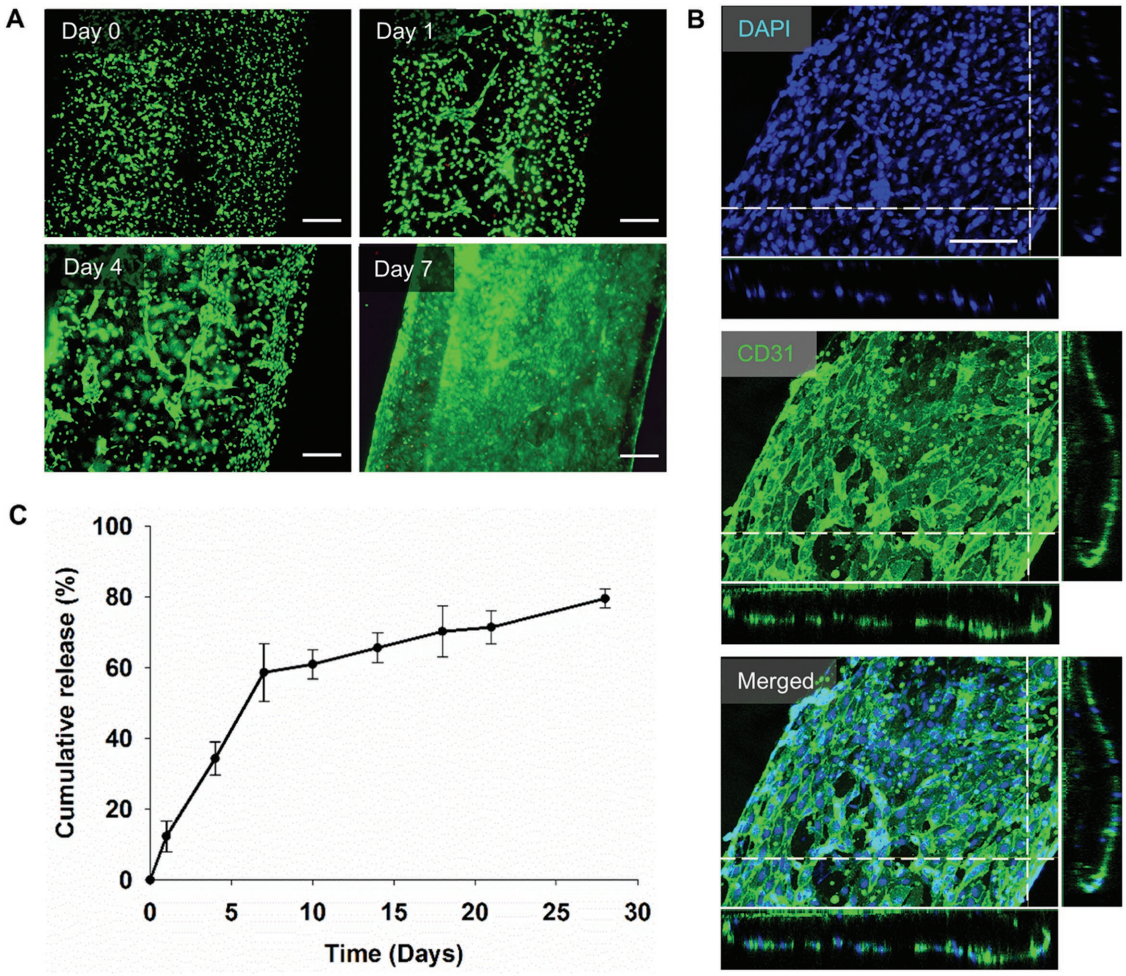


**Figure 5.** The in vitro evaluation of EPC- and APMS-laden BBVs. A) Live/Dead assay for the printed EPC-laden BBV revealed that EPCs maintained high viability after printing and in vitro culturing up to 7 d. B) CD31/DAPI staining indicated that the encapsulated EPCs formed a layer of fully differentiated endothelium on the BBV after culturing for 7 d. C) The cumulative drug release profile showed that the atorvastatin was sustainably released from the BBV carrying AMPS over 28 d.

### 2.4. The In Vitro Performance of the Bio-Blood-Vessel

We fabricated BBV carrying EPCs or APMS of 2 mm length to investigate the in vitro performance such as cellular functions and drug releasing behavior. Approximately 80% of cells were alive immediately after printing (day 0), and the cell viability exceeded 90% after culturing for 1, 4, and 7 d (**Figure 5**A), which indicated that the fabrication condition could maintain cell viability. We stained the EPC-laden BBV against CD31 and connexin 43 antibody to investigate the cell–cell interactions in the printed tubular structure, respectively. The results indicated that the EPCs embedded in the wall of BBV self-organized and formed a monolayer of endothelium with cell–cell attachment (Figure 5B) and interactions (Figure S6, Supporting Information). Although several studies already reported solid filaments covered by the endothelium, none had achieved an endothelialized tubular construct by a direct printing method.[23] To the contrary, hydrogel tubes produced using 3D coaxial cell printing method had never realized endothelialization in the reported studies.[7,8] This observation further substantiates the superiority of our hybrid bioink compared to other ever-applied materials in terms of leveraging printability and biofunctionality for vascular tissue engineering.

An in vitro cumulative release profile illustrated how the drug was sustainably released from printed BBV carrying APMS within a 28 d duration (Figure 5C). We expected that such a continuous elution of atorvastatin would help by constantly improving the performance of EPCs in animal study and eliminating the risk of overdose due to burst release.

### 2.5. Treatment of Ischemic Disease in Mouse Models

To evaluate the therapeutic effect on the ischemic disease, the developed cell/drug laden BBVs were transplanted into a nude mice hind limb ischemia model without surgical anastomosis with the host blood vessels due to its weak mechanical strength. Six experimental groups were applied to in vivo study, including BBV, EPC-laden BBV (EBBV), APMS-laden BBV (ABBV), and EPC/APMS-laden BBV (EABBV), and two


© 2017 The Authors. Published by WILEY-VCH Verlag GmbH & Co. KGaA, Weinheim

control groups (phosphate buffered saline (PBS) injection, and EPC injection). Blood perfusion and limb salvage were assessed to investigate whether BBV-based implants could improve vascular repair in ischemic-injured areas, following the transplantation of the above-mentioned samples into hind limb ischemia BALB/c nude mice. Blood perfusion was assessed by laser doppler perfusion imaging at postoperative days 0, 3, 7, 14, 21, and 28 (**Figure 6**A). The ratio of blood perfusion was significantly higher in the EABBV group compared to the other groups (Figure 6B). In addition, the transplantation of EABBV significantly reduced limb loss, foot necrosis, and toe loss compared to the other groups (Figure 6C,D). Capillary and arteriole densities were quantified by immunofluorescence staining for anti-CD31 (capillary) and anti-alpha smooth muscle actin (anti-$\alpha$-SMA; arteriole) to verify the effect of BBV based implants on neovascularization in ischemic-injured sites. Capillary and arteriole densities were significantly increased upon the transplantation of EABBV, compared to the other groups (Figure 6E–H). These results suggest that the transplantation of EABBV improves neovascularization in ischemic-injured sites.

Immunofluorescence staining was performed on the ischemic thigh at postoperative day 3 to evaluate the survival of transplanted EPCs in the ischemic-injured sites. The apoptosis of the transplanted EPCs was assessed by counting the number of human nuclear antigen (HNA)/cleaved caspase-3 double positive cells (**Figure 7**A). The apoptosis of the transplanted EPCs was significantly decreased in the EBBV and EABBV groups, compared with those in the EPC injection group (Figure 7B). The underlying reason of such increased cell survival lies in that the enhanced cell–ECM interactions contribute to reduce the disassociation of cell and ECM, termed as anoikis. The promoted expression of adhesion molecules (VE-cadherin and integrin beta-1) demonstrated that our bioink can significantly improve the cell–ECM interactions via ECM-mediating signaling (Figure S4, Supporting Information). In addition, loading with atorvastatin increased the survival of transplanted EPCs in ischemic injury sites (Figure 7B). Immunofluorescence staining was performed on ischemic-injured area at postoperative day 28 to investigate the effect of BBV based implants on EPC-mediated endothelial differentiation. Endothelial differentiation of transplanted EPCs was quantified by HNA positive cells in vessels stained with CD31 (Figure 7C). The endothelial differentiation of the transplanted EPCs was significantly increased in the transplantation of EABBV compared with those in other groups (Figure 7D). Treatment with atorvastatin increased the endothelial function through EPC mobilization in ischemic heart failure patients.[3] Atorvastatin facilitates the differentiation of EPC into endothelial cells in mouse carotid arterial injuries.[24] In addition, EPC characteristics are determined by the subjacent matrix.[25] Using synthetic ECM as an EPC delivery vehicle promotes cell survival, engraftment efficiency, endothelial differentiation, and tissue repair.[26] A recent study revealed that ECM proteins enhance the capture of late-outgrowth EPCs under shear flow.[27] These findings indicate that the developed BBV augments the survival and differentiation of transplanted EPCs and atorvastatin represents the synergetic effect on neovascularization in ischemic tissues.

A limitation in the present study is the weak mechanical strength of developed BBV, which hampers its surgical anastomosis with the host blood vessel in the implantation process. We believe this drawback could be overcome through modification of the present BBV to involve an additional shell composed of muscular tissue, which resembles the anatomic feature of its native counterpart. This multiple-layered blood vessel can be potentially realized by designing a triple-coaxial nozzle and modulating the printing parameters. Optimization of the culture conditions for each layer and validation of the interactions among the layers should also be taken into account.

## 3. Conclusion

A major advantage of the developed bioink is its capability of providing a stem cell niche environment in tissue engineered BBVs that have a hollow tube shape. The 3D coaxial cell printing technique allowed us to fabricate BBVs in a broad range of dimensions by adjusting printing parameters. In a nude mouse ischemic model, the EPCs/atorvastatin-laden BBVs promoted the survival and differentiation of EPCs, the neovascularization rate, and salvage of ischemic limbs. These results suggest that our cell/drug-laden BBVs would offer a new therapy for ischemic disorders. In addition, we have demonstrated the perfusion and endothelialization of BBVs during the in vitro stage, which implies its potential application as graft for bypass surgery. Furthermore, the flexibility of 3D cell printing technique would provide BBVs in intricate patterns and predesigned dimensions. In this regard, this platform technique can lead to innovative therapeutic ideas such as opening new avenues for regenerating ischemic diseases, replacing injured blood vessels, direct building prevascularized tissue/organ, and constructing vascular models and biochips.

## 4. Experimental Section

*Cell Culture*: EPCs were isolated from the blood of human umbilical cord as reported previously.[28] Briefly, the total mononuclear cells were isolated by the Ficoll (Thermo Fisher Scientific, Waltham, MA, USA) gradient density centrifugation of human umbilical cord blood. Cells were cultured in EGM-2 MV SingleQuot kit Supplement & Growth Factors (Cat.no. CC-4147, Lonza, Basel, Switzerland) with antibiotic-antimycotic (Cat.no. 15240062, Thermo Fisher Scientific) at 37 °C in 5% $CO_2$. After 4 d in culture, nonadherent cells were removed and fresh culture media were applied. Extended culture was continued until the appearance of spindle-shaped colonies (14–21 d) by refreshing with media. EPCs were cultured in EGM-2 MV SingleQuot kit Supplement & Growth Factors (Lonza) with antibiotic-antimycotic (Cat.no. 15240062, Thermo Fisher Scientific), and incubated at 37 °C in 5% $CO_2$ with the media being refreshed every other day. Once the confluence reached 80%, the cells were washed with PBS (Cat.no. P2200-100, GenDEPOT, TX, USA) twice and detached by incubating with 0.25% Trypsin-EDTA (Cat.no. 59430C, Sigma-Aldrich) for 3 min at 37 °C in 5% $CO_2$. After centrifugation at 1500 rpm for 5 min at room temperature and discarding the supernatants of cell suspension, the cells were resuspended in bioink by gently pipetting.

*Atorvastatin-Loaded PLGA Microspheres*: Atorvastatin-loaded PLGA microspheres were prepared based on the oil-in-water emulsion solvent evaporation technique published elsewhere.[29] Briefly, 120 mg poly(D,L-lactic-*co*-glycolic) acid (Cat.no. 430471, Sigma-Aldrich) and 12 mg atorvastatin calcium salted trihydrate (Cat.no. PZ0001, Sigma-Aldrich) were dissolved in 0.9 mL dichloromethane (Cat.no. 75-09-2, SAMCHUN CHEMICALS, South Korea) to make an organic phase. Then, 180 mg


© 2017 The Authors. Published by WILEY-VCH Verlag GmbH & Co. KGaA, Weinheim

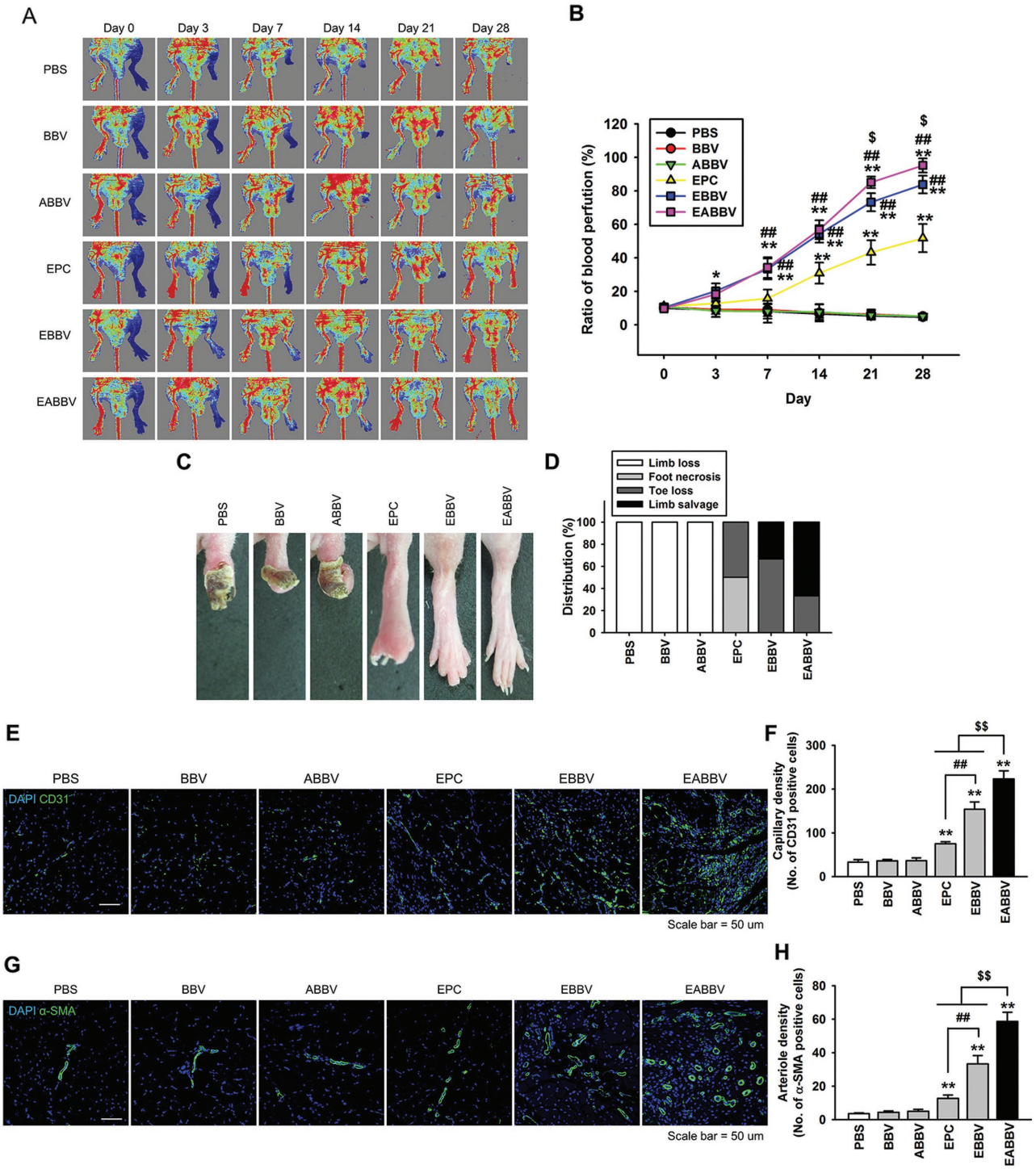


**Figure 6.** The assessment of functional recovery in a murine hind limb ischemia model. A) A murine hind limb ischemia model was established using BalB/c nude mice. The ratio of blood perfusion was evaluated by laser Doppler perfusion imaging analysis in the ischemic limbs of the mice transplanted with PBS, BBV, ABBV, EPCs (EPC), EBBV, and EABBV at 0, 3, 7, 14, 21, and 28 d postsurgery. B) The ratio of blood perfusion (blood flow of the left ischemic limb/blood flow of the right nonischemic limb) was measured. Values represent mean ± SEM. *, $p < 0.05$; **, $p < 0.01$ versus PBS, ##, $p < 0.01$ versus EPC, and $, $p < 0.05$ versus EBBV. C) Representative images illustrating the different outcomes (limb loss, foot necrosis, toe loss, and limb salvage) of ischemic limbs transplanted with six groups at postoperative day 28. D) The distribution of different outcomes in each group at postoperative day 28. E) Ischemic limb tissue samples were immunostained with anti-CD31 antibody (green) for capillary density assessment at postoperative day 28. Scale bar = 50 µm. F) Capillary density was quantified as the number of CD31-positive cells. The values represent mean ± SEM. **, $p < 0.01$ versus PBS, ##, $p < 0.01$ versus EPC, and $$, $p < 0.05$ versus EABBV. G) At postoperative day 28, ischemic limb tissue samples were immunostained with anti-α-SMA antibody (green) for arteriole density assessment. Scale bar = 50 µm. H) Arteriole density was quantified as the number of α-SMA-positive cells. Values represent mean ± SEM. *, $p < 0.01$ versus PBS, ##, $p < 0.01$ versus EPC, and $$, $p < 0.05$ versus EABBV. Abbreviations: BBV, bio-blood-vessel; ABBV, atorvastatin-loaded poly(lactic-*co*-glycolic) acid microspheres (APMS)-laden BBV; EBBV, EPC-laden BBV; EABBV, EPC/APMS-laden BBV.


© 2017 The Authors. Published by WILEY-VCH Verlag GmbH & Co. KGaA, Weinheim

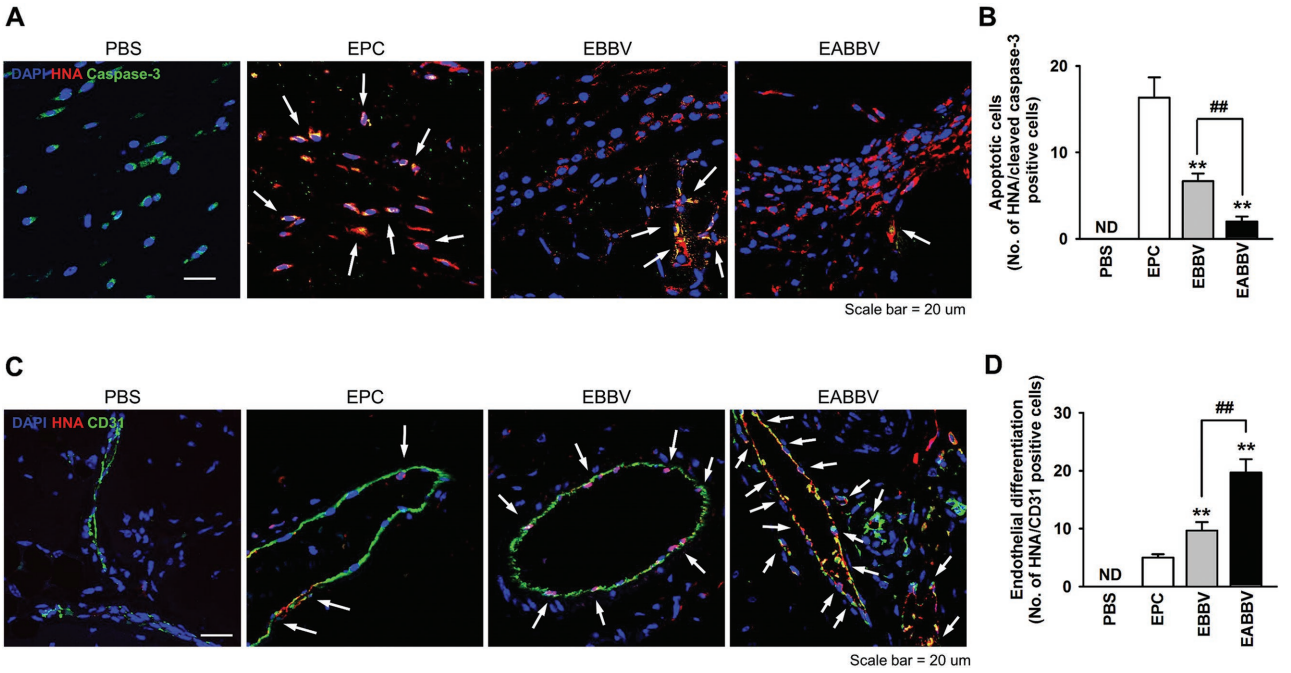


**Figure 7.** EPC/AMPS-laden bio-blood-vessel enhances the survival and endothelial differentiation of transplanted EPCs. A) On postoperative day 3, ischemic injury tissues were assessed to determine the survival of transplanted EPCs. The apoptosis of transplanted cells was analyzed by immunofluorescence staining for anti-human nuclear antigen (HNA, red) and cleaved caspase-3 (Caspase-3, green) antibodies. Scale bar = 20 µm. B) Transplanted apoptotic cells were quantified as the number of HNA- and cleaved caspase-3-positive cells. Values represent mean ± SEM. **, $p < 0.01$ versus EPC, and ##, $p < 0.01$ versus EABBV. C) At postoperative day 28, the endothelial differentiation of transplanted EPCs was assessed by immunofluorescence staining for anti-human nuclear antigen (HNA, red) and CD31 (green) antibodies. Scale bar = 20 µm. D) Endothelial differentiated cells were quantified as the number of HNA- and CD31-positive cells. The values represent mean ± SEM. **, $p < 0.01$ versus EPC, and ##, $p < 0.01$ versus EABBV.

of poly(vinyl alcohol) (PVA) (Cat.no. 363073, Sigma-Aldrich) was dissolved in deionized water to obtain an aqueous phase. The mixture of the two phases was then emulsified using homogenizer (T18 basic ULTRA-TURRAX, IKA, Germany) at 7000 rpm for 120 s. The emulsion was mixed with 50 mL of 0.1 wt% PVA solution and stirred for 4 h to evaporate organic solvents. Subsequently, the emulsion was centrifuged at 4000 rpm and washed three times with deionized water to remove any remaining organic solvents. After freezing at –80 °C overnight and lyophilization for 24 h, the drug-loaded PLGA microspheres were acquired and stored at –20 °C.

*UV Spectrophotometry-Based Quantification*: Identification of the drug content was performed by dissolving 5 mg microspheres in 1 mL acetonitrile (Cat.no. AS017-1, Burdick & Jackson, MI, USA), which was then diluted to 1 mg $mL^{-1}$ using PBS. The precipitated polymer was removed via centrifugation at 12 000 rpm for 10 min. The concentration of atorvastatin in the supernatant was determined by measuring the absorbance at 264 nm against appropriate blank and standards (Epoch2 Microplate Spectrophotometer, BioTek, VT, USA). The atorvastatin content in the microspheres was calculated as

$$\text{Atorvastatin content (\%)} = \frac{W_A}{W_M} \quad (1)$$

Where $W_A$ represents the weight of the quantified atorvastatin, and $W_M$ represents the weight of the atorvastatin-loaded microspheres.

*Decellularization of Vascular Tissue*: The decellularization of vascular tissue was conducted by referring to the protocol published elsewhere with slight modifications.[30] Briefly, the fresh porcine descending aortas of pigs were collected from a local slaughterhouse. Immediately after harvesting, aortas were stored by deep freezing at –80 °C or minced to cubic pieces ≈2 mm in length, followed by washing with deionized water for 6 h to remove any remaining blood. The sliced pieces were then rinsed in 0.3 wt% sodium dodecyl sulfate (Cat.no. 151-21-3, Thermo Fisher Scientific) solution for 24 h and 3 wt% Triton X-100 (Cat.no. 9002-93-1, Sigma-Aldrich) solution for another 24 h with gentle stirring to remove residual cells. After washing out the chemical detergents by treating with PBS for 24 h, the VdECM was deep frozen at –80 °C and lyophilized for 48 h. VdECM hydrogel was prepared by digesting the required amount of VdECM granules in 0.5 M acetic acid solution (Cat.no. 64197, DUKSAN, South Korea) with 10 mg of pepsin (Cat.no. 9001-75-6, Sigma-Aldrich) for 100 mg dECM for 48 h with strong stirring. The VdECM pregel can be stored at 4 °C for at least two months. The effect of decellularization was evaluated using the remaining amount of DNA, collagen, GAGs, and elastin in the decellularized tissue, which were quantitatively assessed and compared with those of native aorta tissue using previously applied methods (Hoechst 33258 assay, hydroxyproline assay, and dimethylmethylene blue assay, elastin quantification assay, respectively).

*Rheological Assessment of Hybrid Bioink*: The hybrid bioink was made using 10 wt% sodium alginate solution, which was first prepared by dissolving alginic acid sodium salt from brown algae (Cat.no. A0682, Sigma-Aldrich) into deionized water, and then mixing with 5 wt% VdECM bioink by strong stirring at 4 °C overnight to obtain a homogeneous solution. After neutralization using 10 M sodium hydroxide (NaOH) (Cat. no. 1310-73-2, SAMCHUN CHEMICALS, South Korea), PBS was added to finalize the hybrid bioink which contains 3% VdECM and 2% sodium alginate (hybrid bioink). Rheological properties were measured using Advanced Rheometric Expansion System (TA Instrument, DE, USA) with 25 mm diameter plate geometry. The viscosities of the collagen hydrogel, VdECM hydrogel, and hybrid bioink were measured by steady shear sweep analysis conducted at 15 °C.

*Biological Evaluation of Hybrid Bioink*: Biocompatibility evaluation was carried out with $1 \times 10^7$ $mL^{-1}$ EPCs encapsulated in hybrid bioink to assess cell viability, proliferation, and differentiation at a certain time. The control was 3% collagen hydrogel prepared with Type-I collagen from porcine skin (Dalim Tissen, South Korea). The cell-entrapped bioink was crosslinked by first treating with $100 \times 10^{-3}$ M calcium chloride ($CaCl_2$) (Cat.no. 07057-00, KANTO CHEMICAL, Japan) solution and then


© 2017 The Authors. Published by WILEY-VCH Verlag GmbH & Co. KGaA, Weinheim

incubating at 37 °C for 30 min. The collagen hydrogel was gelated by incubating at 37 °C for 30 min. Cell viability was checked by staining with a live and dead assay kit (LIVE/DEAD Cell Viability Assay, Thermo Fisher Scientific) following the manufacturer's manual. The cell number was quantified using the cell counting kit-8 assay kit (Cell Counting Kit-8, DOJINDO Molecular Technologies, Japan) following manufacturer's protocol with slight modification to test the cell proliferation rate.

*Cell Proliferation Assay*: The cell proliferation of EPCs following treatment with atorvastatin was assessed by a BrdU Cell Proliferation Assay Kit (Cell Signaling Technology, Danvers, MA, USA) according to manufacturer's instructions.

*Fabrication of BBVs with 3D Coaxial Printing Technique*: A multiple-heads 3D printing system developed in the lab and commercially available coaxial nozzles with series combinations (25G/18G, 19G/15G, 15G/12G, Ramé-Hart Instrument Co., NJ, USA) were used to print the tubular structure. Prior to fabrication, $1 \times 10^7$ $mL^{-1}$ EPCs, and 15 mg $mL^{-1}$ atorvastatin-loaded PLGA microspheres were resuspended in the hybrid bioink neutralized by10 M NaOH, and the pluronic F-127 (Cat.no. P2443, Sigma-Aldrich) was dissolved in $100 \times 10^{-3}$ M $CaCl_2$ solution at a 40 wt% concentration to obtain the fugitive CPF-127 hydrogel. EPC-laden bioink and CPF-127 hydrogel were extruded from the shell and core nozzle with respective pneumatic pressure of 5 and 300 kPa to fabricate the tubular structure. During the printing process, the diffusion of $Ca^{2+}$ ions in CPF-127 hydrogel induces the crosslinking of alginate in bioink to form a tubular structure. Afterward, the samples were submerged in EGM-2 MV media and incubated at 37 °C for 30 min, which led to the dissolution of the CPF-127 hydrogel and the gelation of collagen fibers in bioink.

*Analysis of the In Vitro Drug Releasing Kinetics*: Dialysis was used to measure the cumulative release profile of atorvastatin from fabricated bio-blood-vessels. The printed samples with 517.5 µg atorvastatin were settled in a cellulose dialysis bag (Molecular weight cut-off (MWCO) 3500, Thermo Fisher Scientific) with 3 mL 0.1 M PBS containing 0.01% (w/v) Tween 80 (Cat.no. 9005-65-6, USB, OH, USA). The dialysis bag was suspended in PBS and incubated at 37 °C. At predetermined intervals, 1 mL suspension was collected and the same amount of fresh PBS was supplemented. The mass of released atorvastatin was quantified using a spectrometer (Epoch 2 Microplate Spectrophotometer, BioTek, VT, USA) by checking the absorbance at 264 nm against appropriate standards.[31]

*Murine Hindlimb Ischemia Model*: Experiments were performed on male eight-week-old BALB/c nude mice (Biogenomics, Seoul, Korea) maintained under a 12 h light/dark cycle and in accordance with the regulations of the Pusan National University. All procedures were performed in accordance with the policies of the Institutional Animal Care and Use Committee of the Pusan National University of Korea (IACUC090017). Ischemia was induced by the ligation of the proximal femoral artery and boundary vessels of the mice. No later than 1 h after surgery, experimental groups PBS (PBS injection), EPC (EPC injection), BBV, EBBV, ABBV, and EABBV were transplanted intramuscularly into the ischemic thigh area. Blood perfusion was assessed by comparing the ratio of blood flow in the ischemic limb (left) to that in the nonischemic limb (right) on postoperative days 0, 3, 7, 14, 21, and 28 using laser Doppler perfusion imaging (Moor Instruments, Wilmington, DE, USA).

Other standardized experimental methods are included in the Supporting Information.

## Supporting Information

Supporting Information is available from the Wiley Online Library or from the author.

## Acknowledgements

G.G., J.H.L., and J.J. contributed equally to this work. This study was supported by the National Research Foundation of Korea (NRF) grant funded by the Korea government (MSIP) (No. 2010-0018294) (D.-W.C.) (No. 2015M3A9B4051053, 2015R1A5A2009656, 2015M3A9B4066493) (S.-M.K. and Y.J.H. ), the Basic Science Research Programm through the NRF funded by the Ministry of Education (No. 2015R1A6A3A04059015) (J. J.), the ICT Consilience Creative Program (IITP-R0346-16-1007) supervised by the IITP (Institute for Information & Communications Technology Promotion) (J. J.), and the Korean Health Technology R&D Project, Ministry of Health and Welfare (HI14C2069) (S.-M.K. and Y.J.H.) funded by the Korean government.

## Conflict of Interest

The authors declare no conflict of interest.

## Keywords

3D coaxial cell printing, atorvastatin, decellularized extracellular matrix (dECM), endothelial progenitor cells, vascular tissue engineering

Received: February 13, 2017
Revised: May 14, 2017
Published online: July 19, 2017

[1] T. Asahara, A. Kawamoto, H. Masuda, *Stem Cells* **2011**, *29*, 1650.
[2] a) C. Alev, M. Ii, T. Asahara, *Antioxid. Redox Signaling* **2011**, *15*, 949; b) G. P. Fadini, D. Losordo, S. Dimmeler, *Circ. Res.* **2012**, *110*, 624; c) C. Napoli, T. Hayashi, F. Cacciatore, A. Casamassimi, C. Casini, M. Al-Omran, L. J. Ignarro, *Atherosclerosis* **2011**, *215*, 9; d) P. Chiarugi, E. Giannoni, *Biochem. Pharmacol.* **2008**, *76*, 1352.
[3] E. Oikonomou, G. Siasos, M. Zaromitidou, G. Hatzis, K. Mourouzis, C. Chrysohoou, K. Zisimos, S. Mazaris, P. Tourikis, D. Athanasiou, *Atherosclerosis* **2015**, *238*, 159.
[4] D. Wang, T. Li, H. Wei, Y. Wang, G. Yang, Y. Tian, Z. Zhao, L. Wang, S. Yu, Y. Zhang, *J. Neurol. Sci.* **2016**, *362*, 91.
[5] M.-M. Shi, Y. Kong, Y. Song, Y.-Q. Sun, Y. Wang, X.-H. Zhang, L.-P. Xu, K.-Y. Liu, X.-J. Huang, *Blood* **2016**, *03*, 702803.
[6] J. H. Park, J. Jang, J.-S. Lee, D.-W. Cho, *Ann. Biomed. Eng.* **2017**, *45*, 180.
[7] a) Q. Gao, Y. He, J.-Z. Fu, A. Liu, L. Ma, *Biomaterials* **2015**, *61*, 203; b) Y. Zhang, Y. Yu, A. Akkouch, A. Dababneh, F. Dolati, I. T. Ozbolat, *Biomater. Sci.* **2015**, *3*, 134; c) S. Li, Y. Liu, Y. Li, Y. Zhang, Q. Hu, *Chem. Eng. Process.* **2015**, *95*, 98.
[8] W. Jia, P. S. Gungor-Ozkerim, Y. S. Zhang, K. Yue, K. Zhu, W. Liu, Q. Pi, B. Byambaa, M. R. Dokmeci, S. R. Shin, *Biomaterials* **2016**, *106*, 58.
[9] a) H. C. Ott, T. S. Matthiesen, S.-K. Goh, L. D. Black, S. M. Kren, T. I. Netoff, D. A. Taylor, *Nat. Med.* **2008**, *14*, 213; b) T. W. Gilbert, T. L. Sellaro, S. F. Badylak, *Biomaterials* **2006**, *27*, 3675; c) M. Sawkins, W. Bowen, P. Dhadda, H. Markides, L. Sidney, A. Taylor, F. Rose, S. Badylak, K. Shakesheff, L. White, *Acta Biomater.* **2013**, *9*, 7865; d) D. O. Freytes, J. Martin, S. S. Velankar, A. S. Lee, S. F. Badylak, *Biomaterials* **2008**, *29*, 1630; e) J. M. Singelyn, J. A. DeQuach, S. B. Seif-Naraghi, R. B. Littlefield, P. J. Schup-Magoffin, K. L. Christman, *Biomaterials* **2009**, *30*, 5409; f) Q. W. Tan, Y. Zhang, J. C. Luo, D. Zhang, B. J. Xiong, J. Q. Yang, H. Q. Xie, Q. Lv, *J. Biomed. Mater. Res., Part A* **2017**, *105A*, 1756; g) J. Kundu, A. Michaelson, K. Talbot, P. Baranov, M. J. Young, R. L. Carrier, *Acta Biomater.* **2016**, *31*, 61.
[10] a) F. Pati, D.-H. Ha, J. Jang, H. H. Han, J.-W. Rhie, D.-W. Cho, *Biomaterials* **2015**, *62*, 164; b) J. Jang, H.-J. Park, S.-W. Kim, H. Kim, J. Y. Park, S. J. Na, H. J. Kim, M. N. Park, S. H. Choi, S. H. Park,

 © 2017 The Authors. Published by WILEY-VCH Verlag GmbH & Co. KGaA, Weinheim

*Biomaterials* **2017**, *112*, 264; c) F. Pati, J. Jang, D.-H. Ha, S. W. Kim, J.-W. Rhie, J.-H. Shim, D.-H. Kim, D.-W. Cho, *Nat. Commun.* **2014**, *5*, 3935; d) Y. J. Choi, T. G. Kim, J. Jeong, H. G. Yi, J. W. Park, W. Hwang, D. W. Cho, *Adv. Healthcare Mater.* **2016**, *5*, 2636; e) J. Jang, T. G. Kim, B. S. Kim, S.-W. Kim, S.-M. Kwon, D.-W. Cho, *Acta Biomater.* **2016**, *33*, 88; f) F. Pati, T.-H. Song, G. Rijal, J. Jang, S. W. Kim, D.-W. Cho, *Biomaterials* **2015**, *37*, 230; g) H. Lee, W. Han, H. Kim, D.-H. Ha, J. Jang, B. S. Kim, D.-W. Cho, *Biomacromolecules* **2017**, *18*, 1229.

[11] M. Ehrbar, A. Sala, P. Lienemann, A. Ranga, K. Mosiewicz, A. Bittermann, S. Rizzi, F. Weber, M. Lutolf, *Biophys. J.* **2011**, *100*, 284.

[12] a) K. Hölzl, S. Lin, L. Tytgat, S. Van Vlierberghe, L. Gu, A. Ovsianikov, *Biofabrication* **2016**, *8*, 032002; b) J. Y. Park, G. Gao, J. Jang, D.-W. Cho, *J. Mater. Chem. B* **2016**, *4*, 7521.

[13] a) R. Tiwari, K. Pathak, *J. Pharm. Pharmacol.* **2011**, *63*, 983; b) Y. Naito, T. Terukina, S. Galli, Y. Kozai, S. Vandeweghe, T. Tagami, T. Ozeki, T. Ichikawa, P. G. Coelho, R. Jimbo, *Int. J. Pharm.* **2014**, *461*, 157; c) S. D. Nath, N. T. Linh, A. Sadiasa, B. T. Lee, *J. Biomater. Appl.* **2014**, *28*, 1151.

[14] a) D. J. Hines, D. L. Kaplan, *Crit. Rev. Ther. Drug Carrier Syst.* **2013**, *30*, 257; b) L. Lu, S. J. Peter, M. D. Lyman, H.-L. Lai, S. M. Leite, J. A. Tamada, S. Uyama, J. P. Vacanti, R. Langer, A. G. Mikos, *Biomaterials* **2000**, *21*, 1837.

[15] a) C. Berkland, M. King, A. Cox, K. K. Kim, D. W. Pack, *J. Controlled Release* **2002**, *82*, 137; b) Q. Shang, J. Zhai, R. Tian, T. Zheng, X. Zhang, X. Liang, J. Zhang, *RSC Adv.* **2015**, *5*, 75025.

[16] a) K. W. Chun, H. S. Yoo, J. J. Yoon, T. G. Park, *Biotechnol. Prog.* **2004**, *20*, 1797; b) K. D. Newman, M. W. McBurney, *Biomaterials* **2004**, *25*, 5763.

[17] C. Norotte, F. S. Marga, L. E. Niklason, G. Forgacs, *Biomaterials* **2009**, *30*, 5910.

[18] Y. M. Ju, J. San Choi, A. Atala, J. J. Yoo, S. J. Lee, *Biomaterials* **2010**, *31*, 4313.

[19] a) C. B. Weinberg, E. Bell, *Science* **1986**, *231*, 397; b) Z. H. Syedain, L. A. Meier, J. W. Bjork, A. Lee, R. T. Tranquillo, *Biomaterials* **2011**, *32*, 714.

[20] a) Y. Jung, H. Ji, Z. Chen, H. F. Chan, L. Atchison, B. Klitzman, G. Truskey, K. W. Leong, *Sci. Rep.* **2015**, *5*, 15116; b) N. L'heureux, S. Pâquet, R. Labbé, L. Germain, F. A. Auger, *FASEB J.* **1998**, *12*, 47.

[21] a) L. Dall'Olmo, I. Zanusso, R. Di Liddo, T. Chioato, T. Bertalot, E. Guidi, M. T. Conconi, *BioMed. Res. Int.* **2014**, *2014*, 685426; b) A. Assmann, C. Delfs, H. Munakata, F. Schiffer, K. Horstkötter, K. Huynh, M. Barth, V. R. Stoldt, H. Kamiya, U. Boeken, *Biomaterials* **2013**, *34*, 6015.

[22] D. G. Seifu, A. Purnama, K. Mequanint, D. Mantovani, *Nat. Rev. Cardiol.* **2013**, *10*, 410.

[23] a) H. Onoe, T. Okitsu, A. Itou, M. Kato-Negishi, R. Gojo, D. Kiriya, K. Sato, S. Miura, S. Iwanaga, K. Kuribayashi-Shigetomi, *Nat. Mater.* **2013**, *12*, 584; b) C. Colosi, S. R. Shin, V. Manoharan, S. Massa, M. Costantini, A. Barbetta, M. R. Dokmeci, M. Dentini, A. Khademhosseini, *Adv. Mater.* **2016**, *28*, 677; c) Y. S. Zhang, A. Arneri, S. Bersini, S.-R. Shin, K. Zhu, Z. Goli-Malekabadi, J. Aleman, C. Colosi, F. Busignani, V. Dell'Erba, *Biomaterials* **2016**, *110*, 45.

[24] J. Zhou, L. Chen, Y. Fan, J. Jiang, J. Wan, *Can. J. Physiol. Pharmacol.* **2014**, *92*, 369.

[25] V. Siavashi, S. M. Nassiri, R. Rahbarghazi, R. Vafaei, R. Sariri, *J. Cell. Biochem.* **2016**, *117*, 1934.

[26] P. A. Williams, E. A. Silva, *Ann. Biomed. Eng.* **2015**, *43*, 2301.

[27] J. Zhao, C.-G. Mitrofan, S. L. Appleby, N. W. Morrell, A. M. Lever, *Stem Cells Int,* **2016**, *2016*, 1406304.

[28] J. H. Lee, S. H. Lee, S. H. Choi, T. Asahara, S. M. Kwon, *Stem Cells* **2015**, *33*, 1939.

[29] T.-H. Song, J. Jang, Y.-J. Choi, J.-H. Shim, D.-W. Cho, *Cell Transplant.* **2015**, *24*, 2513.

[30] a) P. J. Schaner, N. D. Martin, T. N. Tulenko, I. M. Shapiro, N. A. Tarola, R. F. Leichter, R. A. Carabasi, P. J. DiMuzio, *J. Vasc. Surg.* **2004**, *40*, 146; b) S. R. Meyer, B. Chiu, T. A. Churchill, L. Zhu, J. R. Lakey, D. B. Ross, *J. Biomed. Mater. Res., Part A* **2006**, *79*, 254; c) Y. Zou, Y. Zhang, *J. Surg. Res.* **2012**, *175*, 359.

[31] A. B. Ahmed, R. Konwar, R. Sengupta, *Braz. J. Pharm. Sci.* **2015**, *51*, 467.


© 2017 The Authors. Published by WILEY-VCH Verlag GmbH & Co. KGaA, Weinheim